Proceedings of the ASME 2010 3rd Joint US-European Fluids Engineering Summer Meeting and 8th International Conference on Nanochannels, Microchannels, and Minichannels
FEDSM-ICNMM2010
August 1-5, 2010, Montreal, Canada

FEDSM-ICNMM2010-31029

THE PENETRATION OF SUBMERGED ROUND TURBULENT GAS JETS IN WATER

Chris Weiland
Virginia Tech Department of Mechanical Engineering

Pavlos Vlachos
Virginia Tech Department of Mechanical Engineering

ABSTRACT

Direct measurements of the interfacial behavior of submerged high speed gas jets with speeds ranging from subsonic to supersonic Mach numbers were performed using high speed digital photography and shadowgraphs. The results indicate that the jets preferentially pinch-off near the axial position which in previous experimental work has been shown to correspond to the location of the maximum streamwise velocity turbulence fluctuations. Using the optical method presented in this paper, the data indicates that the electroresistivity probe technique used by past researchers to quantify the jet penetration into the ambient fluid biases the measurement by up to 30 diameters as the probe cannot identify true jet continuity as opposed to advecting bubbles. We introduce a theoretical jet penetration distance based on a simple force balance of the jet cross-section which compares reasonably well with the measured data. This theoretical jet penetration distance scales with the square of the Froude number and requires an estimation of the jet centerline properties as they evolve downstream of the orifice to accurately predict the pinch-off point. An experimental jet penetration distance is introduced and is defined as the 98.5% contour of the orifice attached gas jet presence over the measurement time.

INTRODUCTION

The problem of jet stability is a classic subject in fluid mechanics [[1]; [2]]. Helmholtz [3], Kelvin [4], and Rayleigh [5] were among the first who laid the mathematical foundations of instability theory governing jets. While the structure and stability of single phase jets have been studied for quite some time [[6]; [7]], multiphase systems formed by a gas jet submerged in liquid are infrequently studied. The submerged gas jet forms a complex multiphase system which is important to the metallurgical [8], chemical [9], and nuclear [10] industries. The metallurgical industry uses submerged gas jets for liquid metal stirring and gas-metal reactions, but it has been shown that if the gas jet enters the bubbling regime close to the gas injection nozzle significant pressure fluctuations on the nozzle tip ensue which tends to cause nozzle erosion. For example, nozzle erosion decreases productivity and efficiency [11]. Thus understanding the conditions that control the stability of the gas jet is important to prolonging the life of the gas injection tip and determining the hydrodynamics and efficiency of the mixing process. These multiphase phenomena are of interest to the nuclear industry for fast breeder reactor technology as the postulated core disruptive accident involves the penetration of nuclear fuel vapor into cold liquid sodium. This interaction has potentially disastrous results for the reactor and thus understanding the dynamics and penetration of the gas jet into the ambient fluid is of utmost importance [12].

Numerous past studies have confirmed the presence of two regimes which characterize the development of the gas flow after leaving the nozzle. At low flow rates the bubbling regime is observed, characterized by the production of bubbles that break near the orifice and rise independently in the direction dictated by gravitational or density effects. A number of studies have concentrated on this regime [[13];[14];[15]]. At higher flow rates a gaseous jet is produced which under some circumstances remains relatively stable and only far downstream of the orifice do bubbles break off from this jet. This study is devoted to the latter regime, namely the study of the characteristics of a submerged high speed gas jet and its transition from a jet to a bubbly plume. Only a small number of previous investigations exploring the physics of these processes are available in the literature.

Identification of a single nondimensional number capable of predicting the transition from bubbling to jetting has dominated the motivation for understanding submerged gas jets. Mori et al [16] was among the first to define a useful quantitative metric to describe the bubbling/jetting transition point. They showed experimentally that the sonic flow region defines the transition point between bubbling and jetting behavior for nitrogen injected into a mercury bath. The bubbling regime

was distinguished from the jetting regime by the fraction of time gas at the orifice had the same diameter as the orifice. McNallan and King [17] studied the effects of several gases (argon, nitrogen, and helium) injected into several liquid baths (water, molten tin, tin-lead alloy, and iron) by high speed photography. They identified the bubbling to jetting transition to occur near the sonic point or more reliably, at a mass flux of 40 g/cm^{2}s which corresponded to the sonic point for all gases but helium. This disparity was not explained. Loth and Faeth [18] conducted measurements on round turbulent gas jets injected vertically into quiescent water at various under-expanded jetting conditions. The under-expansion of a compressible gas jet is due to an imperfectly matched pressure condition at the exit plane of the nozzle. If the nozzle exit pressure is higher or lower than the ambient fluid the flow is termed under-expanded or over-expanded, respectively [19]. Imperfectly expanded jets require some additional process, such as shock or oblique waves, to restore the exhausted gas to the ambient pressure [20]. Using a pitot-probe device, Loth and Faeth measured the presence of a shock cell structure downstream of the orifice. Ito et al [21] sampled the internal flow using a specialized sampling probe to define the slip velocity and entrainment between the two phases. Both the work of Loth and Faeth [18] and Ito et al [21] relied on point measurements of the of the flow field resulting in temporally averaged results to describe the jet.

In trying to define a critical number which dictates the transition from bubbling to jetting, past researchers relied largely on the conventional explanation for the bubbling to jetting transition: the rate of formation of bubbles was such that successive bubbles merged to form a continuous jet and the rate at which bubbles were fractured from this jet was less than their formation rate. More recent explanations for this transition center on hydrodynamic stability theory, namely the Rayleigh-Taylor (RT) and Kelvin-Helmholtz (KH) instabilities and the rate at which instabilities evolve and propagate. Kitscha and Kocamustafaogullari [22] and Zhao and Irons [23] were among the first to identify the importance of such instability mechanisms in dictating the bubbling to jetting transition point and explained that jetting occurs when perturbations travel on the phase boundary faster than they can accumulate. The model of Zhao and Irons [23] compares reasonably well with experimental results. Chen and Richter [24] conducted a thorough perturbation analysis of a compressible gas jet injected into an unbounded inviscid liquid environment. They computed the transonic regime as the bubbling/jetting transition point, and argue the physical mechanism for this behavior as the accumulation of vorticity which is generated by compressibility effects: flow in the subsonic region will have density changes leading to the production of vorticity while the opposite is true in the supersonic regime. This is similar to the classic definition of the KH instability as the stability of a vortex sheath [25] . Jetting is predicted to occur for supersonic gas flows.

Herein we present direct measurements of the interface using shadowgraphs and high speed digital photography. A robust image processing algorithm analyzed the phase boundary from the experimental images. In this paper we employ these measurements to quantify A) the dependence of gas jet pinch-off on Mach number, B) the penetration of submerged gas jets as a function of Mach number, C) the effect of Mach number on interface unsteadiness, and D) the relative importance of the RT and KH mechanisms on the interface motion.

NOMENCLATURE

A – area
AD – average deviation
KH – Kelvin-Helmholtz
L_Q – geometric length scale: $L_Q = \sqrt{A}$
M – Mach number
P – pressure
RT – Rayleigh-Taylor
RMS – root-mean-square
t – time
x – radial position
y – axial position from orifice

Subscripts

e – exit
H - hydrostatic
o – stagnation

EXPERIMENTAL

The experiments were conducted in the Advanced Experimental Thermofluid Engineering Research Laboratory of the Mechanical Engineering Department at Virginia Tech. The experimental setup is shown in Figure 1 and consists of a clear acrylic tank, an injector assembly, pressure and temperature sensors, a fast acting valve which impulsively switched on the gas injection, and a high speed camera which recorded shadowgraph images of the underwater jet. The tests were controlled by a LabVIEW program which simultaneously triggered the high speed camera (Photron APX-RX), monitored various gas pressures and temperatures, and opened the fast acting valve which delivered gas flow to the injector. This allowed for the establishment of an accurate reference time, and synchronization between the sensor and the recorded images. The test matrix is shown in Table 1 where the Reynolds and Richardson numbers are calculated based on the initial (orifice exit) properties. Here P_e refers to the pressure in the exit plane of the nozzle, P_H is the hydrostatic pressure calculated from a barometric load cell and a known water depth, P_o is the stagnation pressure inside the injector, and T_o is the reservoir temperature. The hydrostatic pressure was practically constant across all shots at approximately 1.05×10^5 Pa.

Table 1. Test matrix for all Mach numbers tested. All jets were shot at 0.46m water depth and the properties shown here were calculated for the nozzle exit.

Mach Number	P_e (Pa x10^5)	P_o (Pa x10^5)	P_e/P_H	P_e/P_o	T_o (K)	Mass Flow (kg/s)	Velocity (m/s)	Reynolds No	Richardson No
0.39	1.05	1.16	1.01	0.90	301.7	0.0013	134	3.05E+04	0.035
0.61	1.06	1.37	1.02	0.78	301.8	0.0021	205	4.65E+04	0.0223
0.77	1.09	1.61	1.05	0.67	302.0	0.0029	255	5.78E+04	0.0174
0.91	1.15	1.96	1.10	0.58	301.8	0.0033	294	6.66E+04	0.0144
1.14	1.10	2.46	1.06	0.45	301.3	0.0049	353	8.00E+04	0.0118
1.85	1.08	6.66	1.04	0.16	301.9	0.0145	496	1.13E+05	0.0073

The injectors were composed of a base and a nozzle. Nozzles were rapid prototyped having a constant exit diameter and a varying throat diameter to achieve the desired Mach number. The Mach number was defined in the gas phase only at the exit plane of the nozzle. The nozzles were attached to a base common to all nozzles with several o-rings forming an airtight seal between the base and nozzle. The assembly was flush-mounted to the bottom plate of the acrylic tank. Air was delivered to the nozzle via five gas injection ports evenly spaced about the base. The injectors were submerged in an acrylic tank at a constant depth of 0.46 m with a wave breaker constructed from 3 layers of perforated sheet to limit surface waves and provide a constant hydrodynamic pressure, which was calculated using a Druck PTX-7217 barometric load cell (range: 79–120 kPa absolute, 0.1% full scale accuracy) to measure the atmospheric pressure and a known and closely controlled water depth. Although past researchers have shown that wave dampers do little to change the flow characteristics [[18]; [26]], the wave damper has the added benefit of forcing the ambient waters to reach a stagnant state more quickly after a test.

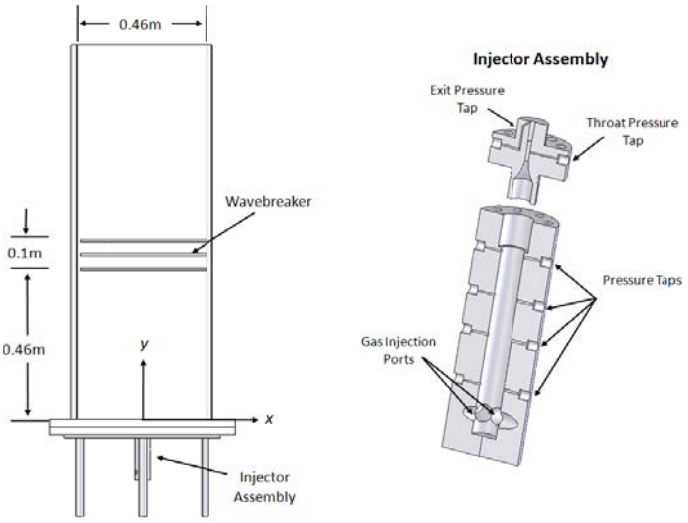

Figure 1. View of the acrylic tank and the injector. The flow pressure was monitored at several points inside the base and at the nozzle throat and exit. Perforated sheets helped to maintain a uniform surface by breaking any large scale surface motions. The injector was flush-mounted to the bottom of the acrylic tank.

Operation and Instrumentation Measurements Details

A schematic illustrating the instrumentation and control system is shown in Figure 2. The system was designed to deliver a constant mass flow to the injector. A pressure reservoir (0.23m^3 volume) was used in conjunction with a gas pressure regulator (Generant model 2GDR-1000B-V-B) that was insensitive to backpressure changes (1.7 kPa output change in flow pressure given 0.69 MPa input change) in reservoir pressure. The pressure downstream of the gas regulator was monitored to ensure a constant delivery pressure. Prior to each test the pressure reservoir was charged from an external gas source until the maximum pressure was attained. The manual valve was then closed to prohibit any line pressure spikes from interfering with the injector gas flow. During a test, the change in the vessel pressure and temperature was monitored to calculate the mass flow rate delivered to the injector using the ideal gas equation. In all cases dried air was used as the working fluid and untreated tap water was used as the quiescent fluid.

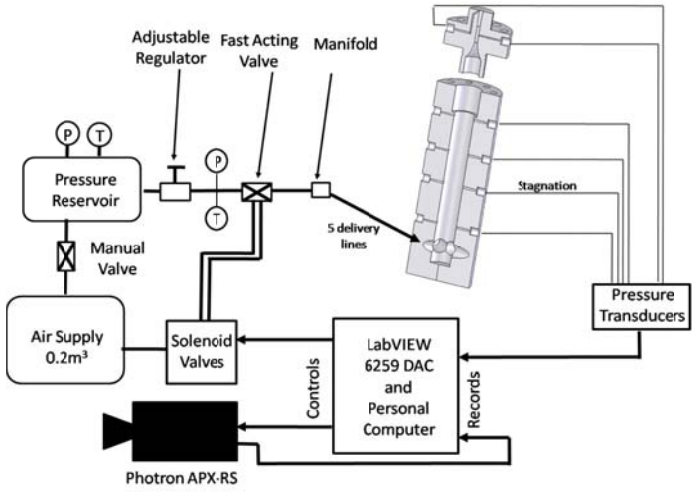

Figure 2. Schematic of the instrumentation and control system. Gas flow is started and stopped using a fast acting pneumatic valve controlled by LabVIEW software, which also triggers all instrumentation.

The system was controlled by LabVIEW software in conjunction with a National Instruments 6259 16-bit DAC. Upon running the software, a low voltage signal is transmitted

to both the Photron camera and a solenoid valve which causes the camera to begin recording and the fast acting valve (W.E. Anderson ¾" NPT, model ABV1DA103) to open simultaneously. The fast acting valve has an opening time of about 0.03s. Not shown in Figure 2 are 10 Clippard (model EV-2-24) solenoid valves controlled by the DAC which deliver compressed gas to the pressure lines while the injector is off. The compressed gas prohibited water intrusion into the pressure lines.

Pressure measurements were taken at a 1 kHz sampling rate with Druck 7217-PTX transducers with an accuracy of 2% full scale. Several ranges of transducers were used to measure signals of different expected pressure ranges in an effort to minimize errors. Temperature measurements were made at the pressure reservoir and just downstream of the adjustable pressure regulator using type K thermocouples with an Omega thermocouple to analog converter (model SMCJ-K) for a total accuracy of +/- 3 deg C. The Mach number was calculated using the isentropic law relating pressure and Mach number. The stagnation pressure was measured at a position several inches downstream of the gas injection ports. Due to propagation of uncertainties in the pressure measurements the error in the Mach number measurements at the nozzle exit was approximately 1% (Mach 1.8) - 7% (Mach 0.4). Considerable effort went into ensuring, in the case of the sonic and supersonic nozzles, that the gas jets were perfectly expanded by monitoring the exit pressure and the known hydrostatic pressure. The experimental pressure ratios are shown Table 1. Values of P_e/P_H=1 indicate a perfectly expanded jet.

Photographic Measurements and Edge Detection

A Photron FASTCAM APS-RX in conjunction with a Canon VX-16 telephoto lens was used to digitally record shadowgraph images of the test section at 1 kHz sampling rate for 14 seconds. The typical magnification used in the tests was approximately 477 μm/pixel. Eight 250W halogen lamps evenly distributed over the test section were arranged behind a white sheet to distribute light evenly over the test section. Acquired images were processed in MATLAB to detect the gas jet boundary in time. As the shadowgraph produces a projection of the gas jet onto a two-dimensional image, no three-dimensional information is collected. The jet boundary is computed using the steps shown in Figure 3. First the image is digitized based on a threshold pixel intensity to distinguish the gas phase from the ambient liquid and a 7x7 pixel median filter is applied to smooth any irregularities such as bubbles fractured from the jet. Next a circular disk morphological element was applied to the digitized image and after dilation and erosion the perimeter of the resulting structure was identified. As shown in Figure 3 the detected boundary agrees quite well with the experimental image. To ensure the nozzle gas flow reached steady-state behavior the jet boundaries were tracked ½ second after the gas jet was initiated. In the context of this work "steady-state" refers to the initial start up jet formed when the gas jet is switched on. All jets had reached the free surface prior to analysis. The computed edges were tracked and their positions recorded for all times which allowed not only the computation of interfacial position, frequencies, velocities, and accelerations but also every pinch-off event in time was identified.

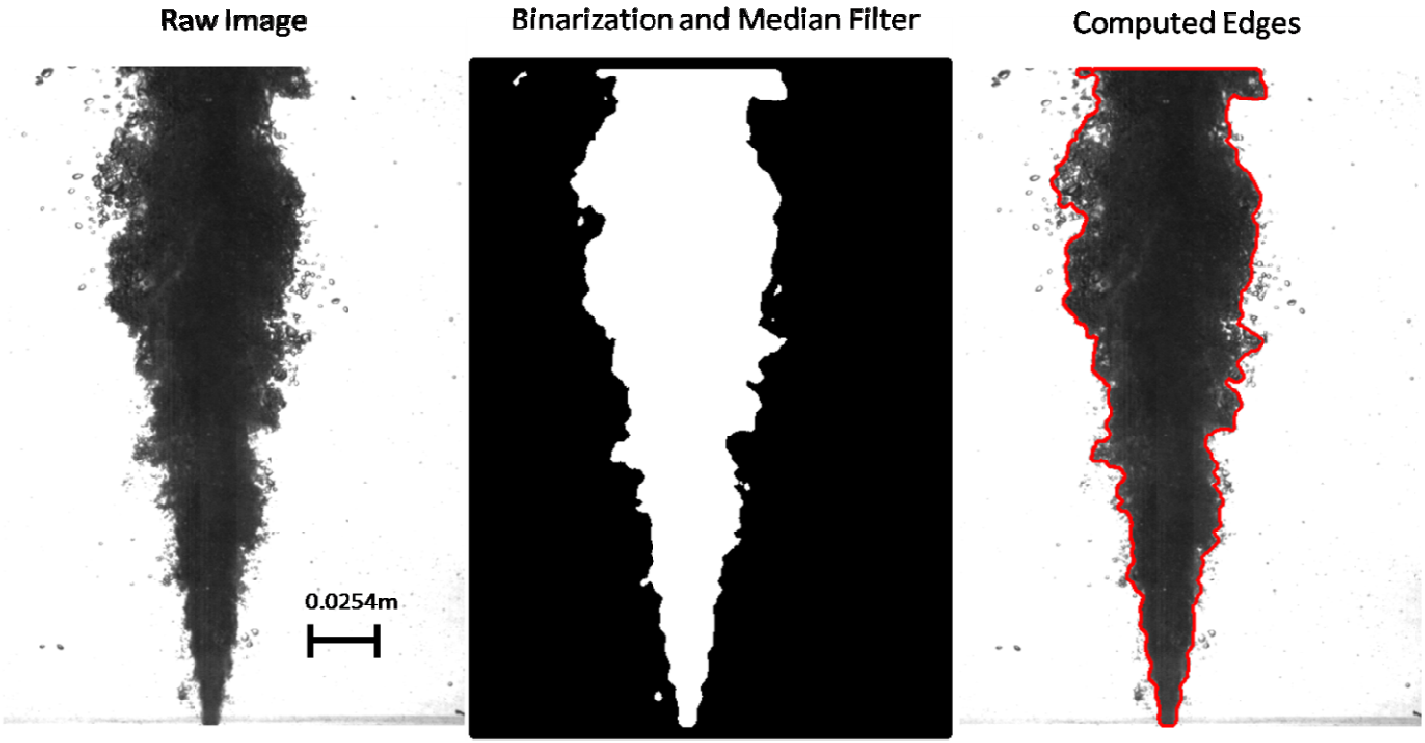

Figure 3. Steps used to detect the jet boundary. The process neglects outliers such as bubbles torn from the interface to accuracy track the phase boundary. The horizontal scale bar represents 0.0254m.

RESULTS AND DISCUSSION

In this paper we employ photographic measurements to quantify A) the dependence of gas jet pinch-off on Mach number, B) the penetration of submerged gas jets as a function of Mach number, C) the effect of Mach number on interface unsteadiness, and D) the relative importance of the RT and KH mechanisms on the interface motion. As far as the authors know, this is the first time quantitative measurements of the entire jet have been attempted to yield insight into global jet properties.

Analysis of Jet Pinch-Off Location

One of the goals of this work was to quantitatively explore the relationship between jet pinch-off and the injection Mach number at a constant hydrostatic pressure. The term pinch-off refers to the state in which the gas jet is no longer continuous from the nozzle to the free surface. The process of events leading up to jet pinch-off is shown in Figure 4 for a Mach 0.8 jet. The jet is considered continuous between 1292ms-1295ms with pinch-off occurring at 1296ms. The jet remains pinched-off in the remainder of the times shown.

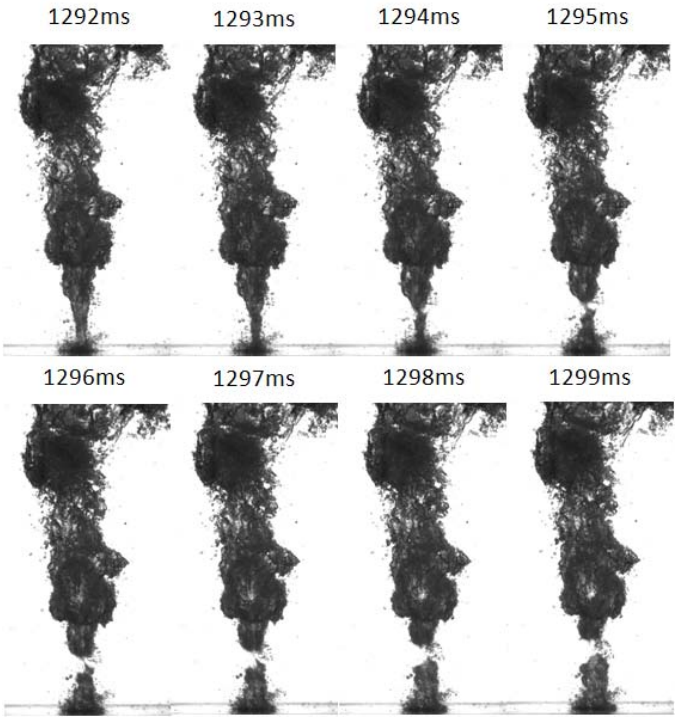

Figure 4. The images show the process of jet pinch-off in a 0.8 Mach jet. The first image is shown 1292ms after the gas jet was begun and subsequent images are shown at 1ms intervals.

The method presented herein builds upon the methods used by past researchers [[8]; [27]] in their determination of jetting or bubbling behavior. To meet this goal the jet interface was tracked using edge detection on high speed digital images as shown in Figure 3. An example of interface tracking at a fixed position 10 diameters downstream of the nozzle exit is shown in Figure 5 for Mach 0.4 and 1.8. One second of time is shown for clarity. Figure 5 shows the position of the interface in time at a fixed distance of 10 diameters downstream from the nozzle exit. The Mach 0.4 jet clearly has several positions, such as approximately 2.63 and 2.73 seconds, where both the left and right interfaces occupy the same radial position. This situation denotes a pinch-off event and this procedure of pinch-off detection was automated in MATLAB.

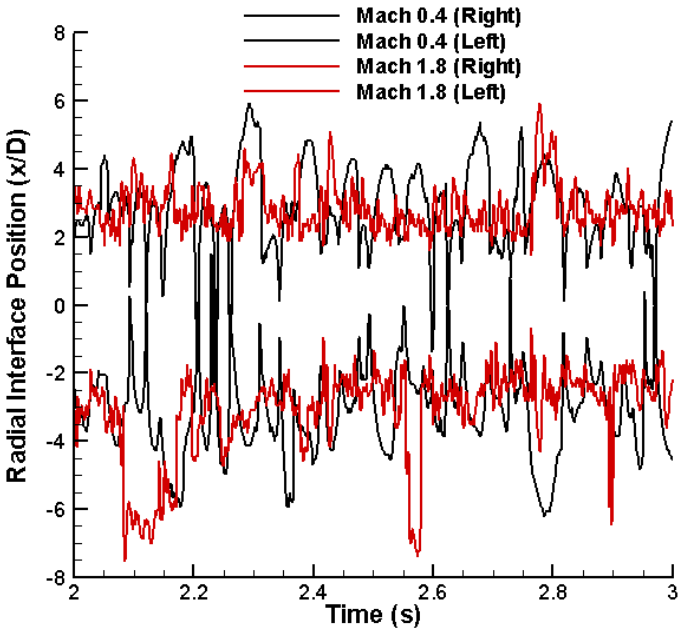

Figure 5. The interface position in time is shown at 10 diameters downstream from the nozzle exit. This information was computed for each test run at each downstream pixel location.

The jet pinch-off locations were recorded and their spatial distribution was determined by summing across all times for each downstream position. The normalized average distribution of pinched-off jet location across three trials for each Mach number is shown in Figure 6 plotted against downstream position y/L_Q. The number of pinch-off measurements is normalized by the maximum number of pinch-off observations that occurred at any point. For example, the Mach 1.1 jet was pinched-off the most at $y/L_Q \approx 14$, and thus the entire Mach 1.1 curve shown was normalized by the number of pinch-off events sustained at $y/L_Q \approx 14$. The location of the pinch-off events is very repeatable for all cases and occurs between $10 < y/L_Q < 15$, with $y/L_Q \approx 14$ corresponding to the peak value location. Mach 0.4 deviates from this behavior demonstrating a broader range of pinch-off locations. This can

be attributed to a more bubbly behavior and as a result the pinch-off location is more distributed.

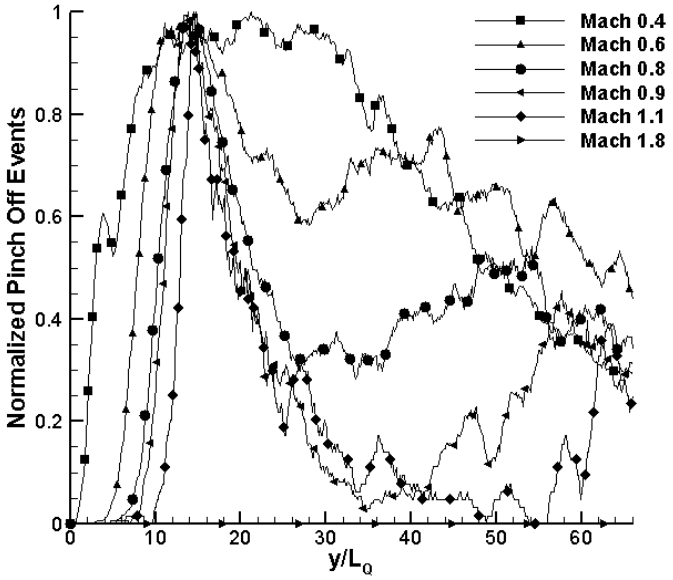

Figure 6. Graph of the average pinch-off location for all Mach numbers. Three trials for each Mach number were averaged to obtain these curves. The Mach 1.8 jet did not pinch-off. All of the jets consistently reached a maximum number of pinch-offs at 10 < y/L_Q < 15.

This finding can perhaps be explained from the internal characteristics of a turbulent gas jet. Although our experiments cannot quantify its internal characteristics, previous research has shown that for single phase jets (i.e. gas jet in gas environment) the streamwise turbulence intensity reaches a peak at $y/L_Q \approx 10$ after which point it steadily decays [[28]; [29]]. This decay point signals the development of self-similar flow. Although our results indicate the maximum number of pinch-offs occurs at a nominal value of $y/L_Q \approx 10$-14 and the literature shows a peak value occurring at $y/L_Q \approx 10$, the similarity between these two values indicates a correlation between pinch-off location and the location of maximum turbulence intensity. This correlation suggests the two may be linked and it is likely that the turbulence acts as a perturbation on the interface to drive its unsteadiness hence leading to pinch-off.

The jet goes through intermittent periods where the jet maintains a continuous presence from the orifice to the free surface, pinch-off where the single jet fractures into multiple independent bubbles, and recovery where pinched-off bubbles re-form into a continuous jet. This behavior is indicative of jetting or bubbling, since by definition a continuous jet cannot pinch-off. This unsteady behavior is quantified by the time interval of continuous jetting and is shown in Figure 7. Here this time interval is plotted against the cumulative time fraction of a continuous jet where the inset shows greater detail over a reduced interval. This Figure not only denotes the total time period for which a gas jet did not pinch-off, but also shows the distribution of time intervals between pinch-off events. The total measurement time was 13.5s. Only pinch-off events lasting 2 ms or more are included as the Nyquist frequency is 500 Hz. For example, the Mach 0.4 jet maintained a continuous presence without pinch-off for about 30% of its life over the time measurement period while the Mach 0.9 and 1.1 jets did not pinch-off for 95% and 96% of the measurement period, respectively. It is readily apparent that the higher Mach numbers have longer periods of jet stability before pinch-off occurs since more time is spent in a longer time interval of continuous jetting behavior. The Mach 1.8 jet never pinched off and therefore is not included in this plot.

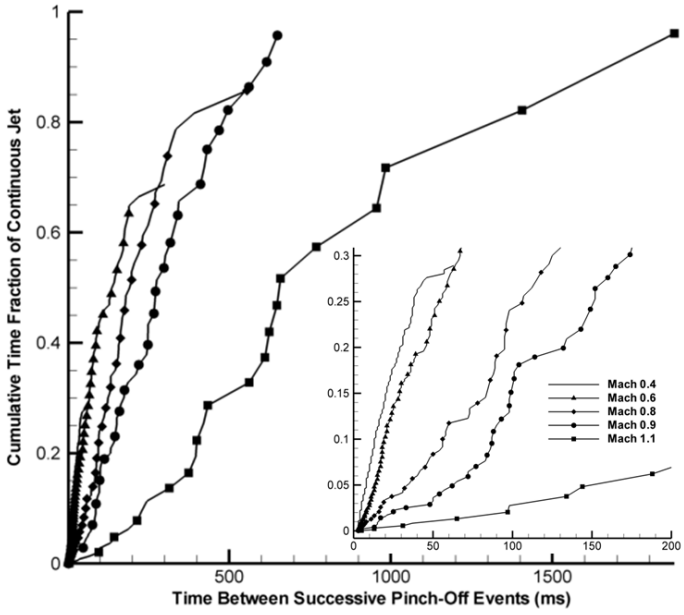

Figure 7. The cumulative time fraction of stable jetting behavior is plotted against the time between successive pinch-offs. The time between successive pinch-off events is indicative of the pinch-off frequency. The inset picture is a zoomed in portion to show greater detail.

The pinch-off frequency can be estimated from the inverse time interval between successive pinch-off events which, as can be seen in Figure 7, occurs over a range of frequencies. The maximum contributor, in terms of time fraction spent at this pinch-off frequency, is shown in Figure 8. The Mach 1.8 jet had a pinch-off frequency of 0 Hz since it never pinched off. The pinch-off frequency drops rapidly as Mach number is increased which is in agreement with Figure 7 and other qualitative observations.

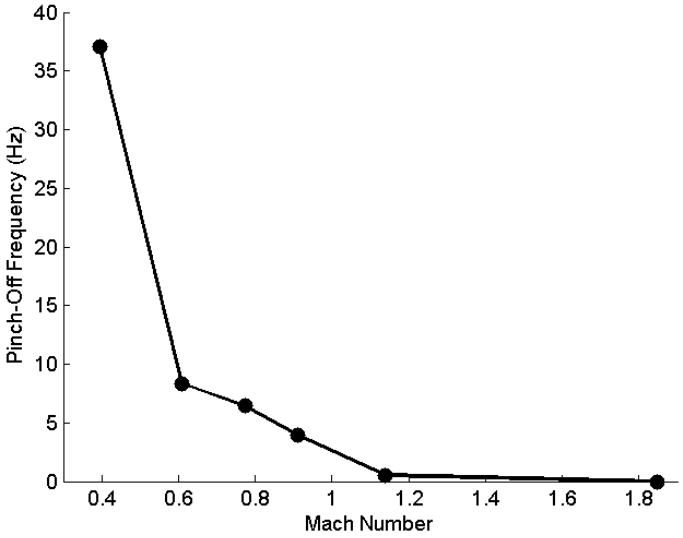

Figure 8. Although it was shown that the jets pinch-off at several frequencies, the jet pinch-off frequency shown here is the largest contributor to the pinch-off phenomenon. The jet pinch-off frequency for Mach 1.8 is 0 Hz as the jet never pinched off.

Jet Penetration Distance

The length of gas jet penetration into the ambient waters is thought to be governed by several parameters, such as the size of the nozzle, the water depth, and Mach number. In the present tests only the variation in jet penetration with Mach number was studied. The jet penetration can only be described statistically as all gas jets pulsate and undulate through their natural motions. Several previous works [[30], [27], and [21]] have measured the mean void fraction using electroresistive or optical probes lowered into the water and traversed through space. Ozawa and Mori [27] use this method to determine what they call gas holdup, which is a statistical mapping of how far gas penetrates into the surrounding waters. If water was present at the measurement point an electrical circuit was completed and registered a value of 1 and if gas was present a value of 0 was recorded. By summing up all of these values in time for many points in space the time fraction of gas penetration at that point was calculated. Here we implement a similar approach but instead we use our non-invasive imaging that measures the position of the gas jet spatially at each instant of time. From the digitized images, as shown in Figure 3, we sum the values of each pixel over time and divide by the measurement duration to arrive at a time fraction of gas presence for all pixel locations as shown in Figure 9 where the color contour indicates the percentage of time that a certain location in the field of view was occupied by gas. A comparison of the Mach 0.4 and Mach 0.9 jets show obvious differences, especially in the length of a gaseous core which occupies a volume for a large percentage of the test record. To quantify and compare this distance between the test cases, we define the jet penetration distance as the maximum centerline location of 98.5% gas occupation averaged over +/- 0.5D about the centerline.

One advantage of this approach is that it enables distinguishing between bubbles that have fractured from the gas jet column and an orifice attached continuous jet, which is not possible using the electroresistive probe. We determine the length of the gas jet penetration only for orifice-attached gas jets, meaning that our calculations ignore any portion of the gas jet that has ruptured and is rising to the surface as an independent bubble.

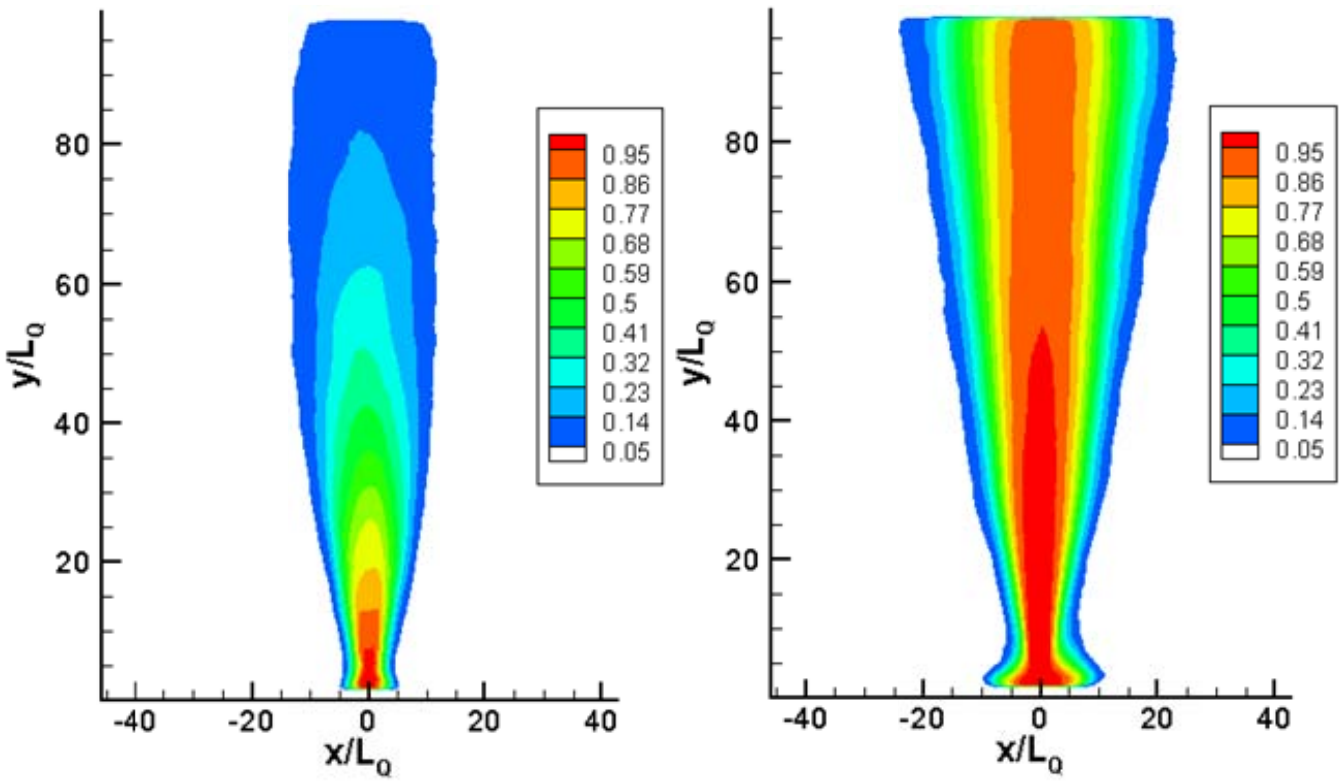

Figure 9. Gas holdup contours for a Mach 0.4 jet (left) and Mach 0.9 jet (right). The gas holdup is a statistical mapping of how far gas penetrates into the surrounding waters. The transonic gas jet penetrates further into the quiescent fluid statistically than the subsonic gas jet.

Both the experimental results from this work and the predicted jet penetration distances are shown in Figure 10. The vertical bars represent repeatability across the three trials for each Mach number. The penetration distance including only orifice-attached jets that neglect independent bubbles which have fractured from the gas jet is shown in Figure 10 as open circles. The penetration distance is also computed from the experimental data to simulate the response of an electroresistivity probe by including bubbles that have pinched off from the gas jet and are rising independently and is shown with open squares. The orifice attached only jets have a smaller penetration distance than when also considering pinched-off bubbles in the measurement, and it is apparent that electroresistivity probes over-estimate the gas jet penetration, particularly at larger Mach number flows.

Figure 10 also compares two metrics for delineating between bubbly and jetting flows. The method utilized in this work uses the measured jet penetration using orifice attached jets only and is shown with open circles. The 'x' symbols show the average interface position at 0.8 mm (y/L_Q=0.14) downstream of the orifice plotted against the Mach number. The former metric was defined in this paper and the latter has been used as a metric to define jetting/bubbling behavior in a past work [16]. Consider Figure 8, which clearly shows that as the Mach number increases the flow becomes more jet like since the frequency at which the gas jet pinches off decreases. As shown in Figure 10 the jet penetration length appears to be a better metric for denoting bubbling or jetting behavior, as the average jet diameter near the orifice shows the Mach 0.4 and Mach 1.8 jets to have a similar jet radius near the orifice: the average interface position for the Mach 1.8 jet is x/L_Q=1.05 at a pinch-off frequency of 0 Hz while the Mach 0.4 jet has an average orifice position of approximately x/L_Q=1 with a pinch-off frequency of about 37 Hz. Between these Mach numbers the average interface position increases and then decreases, even though the pinch-off frequency is decreasing (Figure 8). The jet penetration metric shows the jet penetration distance to be decreasing with increasing pinch-off frequency, which corresponds with experimental observations and the results presented here.

The reason the latter metric is less effective is because while some jets can maintain a significant presence at the orifice, and would thus be labeled as jetting, they tend to pinch-off further downstream exhibiting clear bubbly flow behavior. Thus a global measurement technique, such as the optical method presented in this paper, is required to capture this effect. Consider the Mach 0.6 and 0.8 curves in Figure 6 which, although they exhibit distinctive peaks in the pinch-off location at $y/L_Q \approx 14$, also include pinch-off locations downstream of $y/L_Q \approx 14$. Obviously this cannot be captured by electrodes at the orifice only, which therefore cannot capture the true dynamics of the flow. Of course, the optical method presented in this

work requires the ambient fluid to be optically clear which would be impossible when working with liquid metal baths.

The jet penetration distance measured by the simulated electroresistivity probe technique appears to indicate an inflection point near or at the sonic point, but it is unclear if this is in agreement with the actual (orifice attached) penetration distance due to a lack of Mach numbers tested between 1.1 and 1.8. The Mach 1.8 jet is predicted to never pinch-off as the penetration distance is longer than the imaging domain which is in agreement with the experimental results over the limited depths observed.

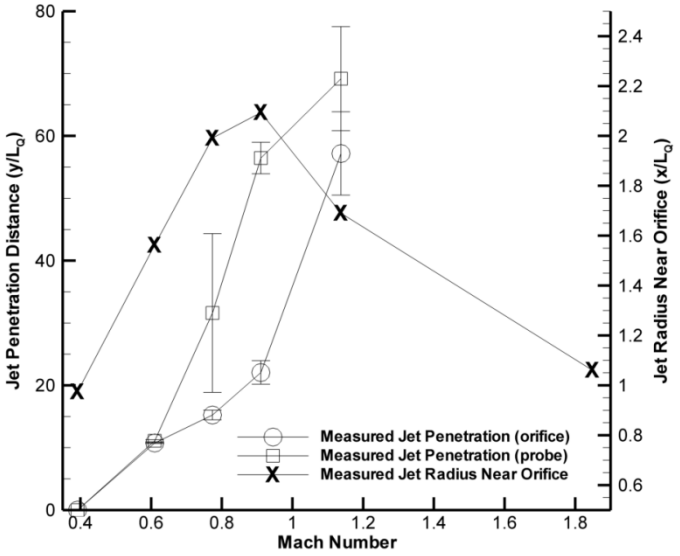

Figure 10. The jet penetration distance is calculated using only the jet attached to the orifice (circle) and including bubbles advected downstream (square). The Mach 0.4 jet did not maintain a permanent penetration distance 98.5% of the measurement time and the Mach 1.8 jet never pinched off in the measurement domain (penetration length of at least 91 y/L_Q).

Unsteady Interface Characteristics

The average deviation (AD) of the interface radial position was calculated along the jet for all locations where the jet maintained a presence for 80% of the recorded time over a period of 13.5s and is shown in Figure 11. The signal was mean-removed prior to calculating the AD values and thus only the unsteadiness of the interface was computed. The results indicate that downstream positions yield more interfacial unsteadiness while larger Mach numbers yield less interfacial unsteadiness.

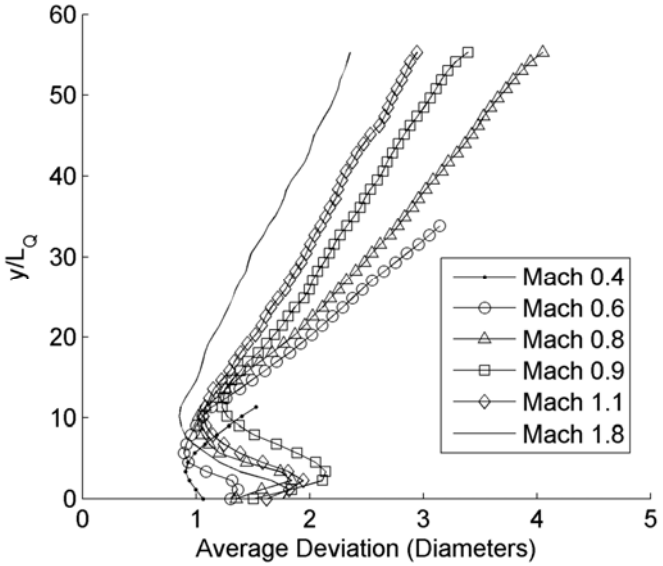

Figure 11. In general, the interface unsteadiness increases downstream and decreases for higher Mach numbers. The average deviation calculation was only performed on locations which were not pinched-off for 80% of the total recorded time.

Further analysis of the interfacial unsteadiness shows that at approximately $y/L_Q \approx$ 10-11 Mach numbers 0.6, 0.8, 0.9, and 1.1 undergo a switch in their trends of interfacial unsteadiness. Prior to this location the Mach 0.9 and 1.1 jets have higher unsteadiness but downstream of this point the subsonic Mach numbers have higher unsteadiness. The Mach 0.4 and 1.8 jets do not follow this trend, as the Mach 0.4 jet rapidly overtakes all other jets at $y/L_Q \approx 10$ and the Mach 1.8 jet has the lowest unsteadiness after $y/L_Q \approx 8$. It is readily apparent from these and previously described observations that Mach 0.4 corresponds to a bubbly flow as opposed to a jetting flow. Given the switch in interfacial behavior for almost all of the Mach numbers at $y/L_Q \approx$ 10-11, this position appears to be the jet development length described for single phase jets [[28]; [29]], although in the present experiment we cannot confirm whether this development length is due to internal turbulence levels, compressibility effects, or some other phenomena.

The second observation is that the transonic and supersonic gas jets may have higher unsteadiness near the orifice due to compressibility effects. The presence of a shock cell structure in submerged gas jets was confirmed experimentally by Loth and Faeth [18] through static pressure measurements just downstream of the orifice. As the interface rapidly expands and contracts near the orifice, this character is felt downstream in the form of a propagating interfacial wave. If the propagating interfacial wave is large enough in amplitude it will induce large interfacial motions which can lead to pinch-off. In the case of transonic and supersonic jets, the rapid oscillation of the gas-liquid interface near the orifice quickly generates a bubbly flow through the Rayleigh-Taylor instability. It is plausible that this bubbly flow surrounding the gas jet near the orifice acts as a damping mechanism to lessen subsequent impulsive

oscillations of the interface, which in turn propagates a wave of smaller amplitude downstream. The subsonic gas jets, on the other hand, tend to exhibit low frequency oscillations which do not produce this damping mechanism, and thus all interfacial motions are propagated downstream where they contribute to the overall unsteadiness of the interface.

The third observation is that a maximum in interfacial unsteadiness occurs near the sonic point at $y/L_Q \approx 4.5$ which then decreases in the supersonic region. This result seems to corroborate the work of Chen and Richter [24] in a qualitative sense as 1) they computed the bubbling to jetting transition to occur at the sonic point and as indicated by the upper subset picture in Figure 10 a large jump appears in the gas jet penetration length with a subsequent decrease in the number of pinch-off events in the supersonic regime and 2) they computed that a maximum in the axisymmetric temporal and spatial growth rates occur at the sonic point and which then quickly reduce at supersonic Mach numbers. Although in this work we do not compute growth rates we can infer interface stability based on the unsteadiness of the interface. Here the term stability is loosely defined by the motion of the interface; a perfectly stable interface is composed of a slowly diverging column of gas rising from the orifice to the free surface with no motion of the interface. Thus it follows that as the interface AD values become smaller the jet approaches a perfectly stable interface. Based on this interpretation, the sonic point does appear to be the least stable Mach number. Additionally, if the interface unsteadiness can be linked to stability, then the slope of the AD versus downstream position is indicative of the spatial instability growth rate. As shown in Figure 11 for $y/L_Q > 10$ the slope decreases with increasing Mach number, indicating increasing Mach number yields more stable jets with lower growth rates.

Although stability and the unsteady interface motions reported here are fundamentally different they are phenomenologically similar. This is apparent from the results reported here as increased interfacial motions are experimentally correlated to a less stable jet exhibiting a greater number of pinch-off events. The interface unsteadiness was quantified by calculating the average deviation (AD) of the entire interface position as was shown in Figure 11. Thus, the growth of the interface unsteadiness as it evolves axially may be linked to the spatial growth rate of the interface unsteadiness. The growth rate is presented in Figure 12 for all Mach number flows. These were calculated by fitting a line to each AD curve shown in Figure 11. The slope of each line denotes the growth rate as this was the rate at which the interfacial unsteadiness increased. The line was fitted after the inflection point of each AD curve to ensure the jet was fully developed. For example, the growth rate for the Mach 1.8 test was calculated from the slope of the best fit line fitted over the interval $10 \leq y/L_Q \leq 55$. The results shown in Figure 12 indicate a steadily decreasing spatial growth rate as Mach number increases. These results are somewhat in agreement with the calculations of Chen and Richter [24], who computed both the temporal and spatial growth rates for an air jet submerged in water. Although they compute the supersonic regime to be the most stable which is in agreement with the results shown here, they computed a steadily increasing growth rate up to the sonic point which is clearly not seen here. The reason for this discrepancy is not clear, although Chen and Richter [24] assumed an idealized interface with no mixing which is not realized here.

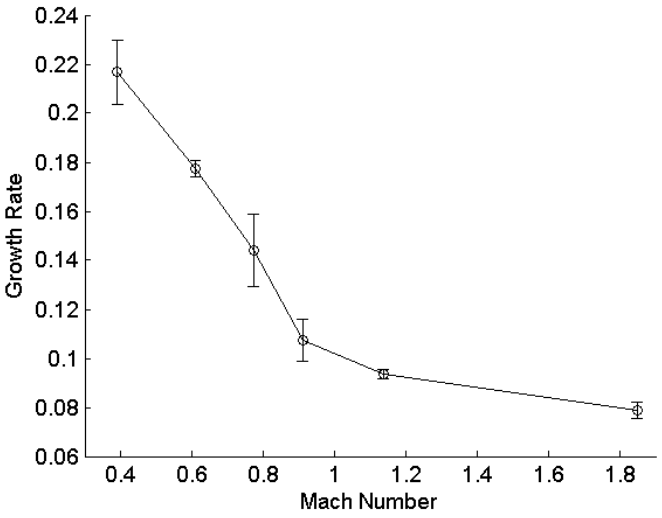

Figure 12. The spatial growth rate decreases with increasing Mach number. The growth rate is a nondimensional scale representing the rate of interface unsteadiness downstream and is given by the slope of the best fit line passing through the AD points.

CONCLUSIONS

Direct measurements of the interfacial behavior of submerged high speed gas jets ranging from subsonic to supersonic Mach numbers were performed using high speed digital photography. While past researchers have relied on pressure history at the injection point or electrode contact circuits to determine the jetting/bubbling transition point, as far as the authors know, this work is the first to directly measure the entire interface in both space and time simultaneously. Of course, the method presented in this paper requires the ambient fluid to be optically clear. There are several main conclusions of this work:

1. Buoyant jets were observed to consistently pinch-off at a spatial location corresponding to the maximum axial velocity turbulence fluctuations, namely on the interval $10 < y/L_Q < 15$. This suggests that buoyant jets are very sensitive to the internal turbulence levels, which experiments have shown reach a peak at $y/L_Q \sim 10$ in single phase jets.
2. The electroresistive probe technique used by many researchers to establish a jet penetration distance inherently biases the measurement by as much as 30 diameters. This is due to the probe technique not distinguishing between orifice attached jets – crucial to the definition of jetting – and bubbles which break from the jet and advect upwards.

3. The jet penetration distance defined in this paper is an improved metric for defining jetting as opposed to the bubble diameter at the orifice. A simple force balance on the gas jet based on measurements by others agrees reasonably well with the experimentally measured jet penetration distance. The classic jetting length L_M does not perform well for estimating this distance for buoyant gas jets.
4. The jet unsteadiness near the orifice is a function of the Mach number and reaches a peak near the sonic point suggesting that these are the least stable in terms of interfacial motion. The sonic point was observed to be the bubbling/jetting transition point as the jet penetration distance increased markedly after this point. The spatial instability growth rate was shown to decrease as the Mach number was increased.

ACKNOWLEDGEMENTS

This research was sponsored by the Naval Surface Warfare Center, Dahlgren Division. Mr. John Busic and Dr. Jon Yagla served as the technical monitors. Their support is gratefully acknowledged.

REFERENCES

[1] Lin, C. C., and Benney, D. J., 1962, "On the Instability of Shear Flows," Proc. Sym. App. Math, 13(pp. 24.
[2] Birkhoff, G., 1962, "Helmholtz and Taylor Instability," Proc. Sym. App. Math, 13(pp. 21.
[3] Helmholtz, H. V., 1868, "On Discontinuous Movements of Fluids," Phil. Mag., 36(4), pp. 9.
[4] Kelvin, W., 1871, "Hydrokinetic Solutions and Observations," Phil. Mag., 42(4), pp. 15.
[5] Rayleigh, J., 1879, "On the Instability of Jets," Proc. Lond. Math. Soc., 10(pp. 10.
[6] Dimotakis, P. E., Miakelye, R. C., and Papantoniou, D. A., 1983, "Structure and Dynamics of Round Turbulent Jets," Physics of Fluids, 26(11), pp. 3185-3192.
[7] Wang, H. W., and Law, A. W. K., 2002, "Second-Order Integral Model for a Round Turbulent Buoyant Jet," Journal of Fluid Mechanics, 459(pp. 397-428.
[8] Wraith, A., and Chalkly, M., 1977, Advances in Extractive Metallurgy, IMM, London,
[9] Darmana, D., Deen, N. G., and Kuipers, J. a. M., 2005, "Detailed Modeling of Hydrodynamics, Mass Transfer and Chemical Reactions in a Bubble Column Using a Discrete Bubble Model," Chemical Engineering Science, 60(12), pp. 3383-3404.
[10] Chawla, T. C., 1975, "Rate of Liquid Entrainment at Gas-Liquid Interface of a Liquid Submerged Sonic Gas Jet," Nuclear Science and Engineering, 56(1), pp. 1-6.
[11] Sahai, Y., and Guthrie, R. I. L., 1982, "Hydrodynamics of Gas Stirred Melts .1. Gas-Liquid Coupling," Metallurgical Transactions B-Process Metallurgy, 13(2), pp. 193-202.
[12] Epstein, M., Fauske, H., Kubo, S., Nakamura, T., and Koyama, K., 2001, "Liquid Entrainment by an Expanding Core Disruptive Accident Bubble - a Kelvin/Helmholtz Phenomenon," Nuclear Engineering and Design, 210(pp. 24.
[13] Brodkey, R. S., 1967, *The Phenomena of Fluid Motions*, Dover,
[14] Ruzicka, M. C., Drahos, J., Zahradnik, J., and Thomas, N. H., 1997, "Intermittent Transition from Bubbling to Jetting Regime in Gas-Liquid Two Phase Flows," International Journal of Multiphase Flow, 23(4), pp. 671-682.
[15] Cieslinski, J. T., and Mosdorf, R., 2005, "Gas Bubble Dynamics - Experiment and Fractal Analysis," International Journal of Heat and Mass Transfer, 48(9), pp. 1808-1818.
[16] Mori, K., Ozawa, Y., and Sano, M., 1982, "Characterization of Gas-Jet Behavior at a Submerged Orifice in Liquid-Metal," Transactions of the Iron and Steel Institute of Japan, 22(5), pp. 377-384.
[17] Mcnallan, M. J., and King, T. B., 1982, "Fluid-Dynamics of Vertical Submerged Gas Jets in Liquid-Metal Processing Systems," Metallurgical Transactions B-Process Metallurgy, 13(2), pp. 165-173.
[18] Loth, E., and Faeth, G. M., 1989, "Structure of Underexpanded Round Air Jets Submerged in Water," International Journal of Multiphase Flow, 15(4), pp. 589-603.
[19] Shapiro, A., 1953, *The Dynamics and Thermodynamics of Compressible Fluid Flow*, John Wiley & Sons, New York.
[20] Liepmann, H., and Roshko, A., 1957, *Elements of Gasdynamics*, John Wiley & Sons, New York.
[21] Ito, K., Kobayashi, S., and Tokuda, M., 1991, "Mixing Characteristics of a Submerged Jet Measured Using an Isokinetic Sampling Probe," Metallurgical Transactions B-Process Metallurgy, 22(4), pp. 439-445.
[22] Kitscha, J., and Kocamustafaogullari, G., 1989, "Breakup Criteria for Fluid Particles," International Journal of Multiphase Flow, 15(4), pp. 573-588.
[23] Zhao, Y. F., and Irons, G. A., 1990, "The Breakup of Bubbles into Jets During Submerged Gas Injection," Metallurgical Transactions B-Process Metallurgy, 21(6), pp. 997-1003.
[24] Chen, K., and Richter, H. J., 1997, "Instability Analysis of the Transition from Bubbling to Jetting in a Gas Injected into a Liquid," International Journal of Multiphase Flow, 23(4), pp. 699-712.
[25] Batchelor, G. K., 1967, *An Introduction to Fluid Dynamics*, Cambridge University Press,
[26] Dai, Z. Q., Wang, B. Y., Qi, L. X., and Shi, H. H., 2006, "Experimental Study on Hydrodynamic Behaviors of High-Speed Gas Jets in Still Water," Acta Mechanica Sinica, 22(5), pp. 443-448.
[27] Ozawa, Y., and Mori, K., 1986, "Effect of Physical-Properties of Gas and Liquid on Bubbling Jetting Phenomena in Gas Injection into Liquid," Transactions of the Iron and Steel Institute of Japan, 26(4), pp. 291-297.
[28] Crow, S. C., and Champagne, F. H., 1971, "Orderly Structure in Jet Turbulence," Journal of Fluid Mechanics, 48(03), pp. 547-591.

[29] Fischer, H., List, E., Koh, R., Imberger, J., and Brooks, N., 1979, *Mixing in Inland and Coastal Waters*, Academic Press, New York.
[30] Castillejos, A. H., and Brimacombe, J. K., 1987, "Measurement of Physical Characteristics of Bubbles in Gas-Liquid Plumes .1. An Improved Electroresistivity Probe Technique," Metallurgical Transactions B-Process Metallurgy, 18(4), pp. 649-658.